Journal of Fluids and Structures 41 (2013) 9–21

Contents lists available at ScienceDirect

Journal of Fluids and Structures

journal homepage: www.elsevier.com/locate/jfs

The flow past a circular cylinder translating at different heights above a wall

A. Rao [a,*], M.C. Thompson [a], T. Leweke [b], K. Hourigan [a,c]

[a] Fluids Laboratory for Aeronautical and Industrial Research (FLAIR), Department of Mechanical and Aerospace Engineering, Monash University, Clayton 3800, Australia
[b] IRPHE UMR 7342, CNRS, Aix-Marseille Université, 13384 Marseille, France
[c] Division of Biological Engineering, Monash University, Clayton 3800, Australia

ARTICLE INFO

Article history:
Received 30 March 2012
Received in revised form
6 August 2012
Accepted 19 August 2012
Available online 17 October 2012

Keywords:
Wakes
Stability analysis
Body forces
Flow transition

ABSTRACT

The flow past a circular cylinder moving through a fluid at different heights above a plane no-slip boundary is investigated numerically for Reynolds numbers $\lesssim 200$. The gap height is varied from large values, effectively corresponding to the freestream case ($G/D=\infty$), down to a small value where the cylinder is just above the wall ($G/D=0.005$). The initial transition from steady two-dimensional flow can occur through either a Hopf bifurcation to unsteady flow or through a regular bifurcation to steady three-dimensional flow. The critical Reynolds numbers for each case are determined as a function of gap height. It is found that steady two- to three-dimensional transition occurs first at gap ratios $G/D \lesssim 0.25$, beyond which the initial transition is to unsteady flow. At $G/D=0.3$, a sharp increase in the critical Reynolds number is observed at which three-dimensionality occurs. On increasing gap height, the critical Reynolds number initially decreases before again increasing towards the value observed for an isolated cylinder. The force coefficients and Strouhal numbers are quantified. Finally, three-dimensional simulations are performed at $\mathrm{Re}=200$ for the smallest gap ratio, effectively corresponding to a cylinder sliding along a wall, to examine how the wake evolves as it saturates.

1. Introduction

The flow past a circular cylinder has represented a generic fluid flow problem for more than a century, and the experimental and mathematical details of the transition to three-dimensional flow have been revealed over the last 25 years. The flow undergoes an initial transition from two-dimensional periodic flow to three-dimensional flow via a sub-critical transition at $\mathrm{Re} \simeq 190$ (Barkley and Henderson, 1996; Williamson, 1996a, 1996b), where the Reynolds number (Re) is based on the free-stream velocity (U) and the cylinder diameter (D). The spanwise modulation of this three-dimensional flow at onset was found to be approximately four cylinder diameters and the corresponding wake instability is commonly known as the *Mode A* instability. Another three-dimensional instability mode, *Mode B*, becomes unstable at a higher Reynolds number and the remnants of that mode seem to persist to much higher Reynolds numbers as the wake undergoes a transition to a chaotic state (Henderson, 1997; Williamson, 1996a, 1996b). The equivalent modes have also been recognised in the wakes of other two-dimensional cylindrical bodies, such as square cylinders (Robichaux et al., 1999)

* Corresponding author.
E-mail address: anirudh.rao@monash.edu (A. Rao).

0889-9746/$ - see front matter © 2012 Elsevier Ltd. All rights reserved.
http://dx.doi.org/10.1016/j.jfluidstructs.2012.08.007

and elongated cylinders (Ryan et al., 2005). Until recently, very few studies have investigated the related problem of flow past a circular cylinder moving parallel to a wall and the associated wake transitions.

Bearman and Zdravkovich (1978) performed experimental investigations for a cylinder near a fixed wall at $Re = 4.5 \times 10^4$ for $0 \le G/D \le 3.5$. The cylinder was located $36D$ from the start of a turbulent boundary layer which developed along the wall. They observed the suppression of regular vortex shedding for $G/D < 0.3$, with the Strouhal number remaining almost constant until this gap height was approached.

Price et al. (2002) visualised the flow for a circular cylinder at different gap heights from a fixed wall for Reynolds number in the range of $1200 \le Re \le 4960$ and identified four different regimes of flow. For the case where the cylinder was close to the wall ($G/D < 0.125$), vortex shedding was suppressed and the wall boundary layer separation occurred both upstream and downstream of the cylinder. For $0.25 \le G/D \le 0.375$, the flow was qualitatively similar to that for the small gap ratios, while pairing occurred between the inner shear layer from the cylinder and the wall boundary layer. Vortex shedding was detected for $G/D > 0.5$, and at higher gap heights, the flow resembled that of an isolated cylinder.

Experimental investigations undertaken by Bailey et al. (2002) for a square cylinder near a stationary wall at $Re = 1.89 \times 10^4$ showed the presence of dislocations (which are commonly associated with mode A type instability) for gap heights greater than $G/D = 0.7$. For $0.53 \le G/D \le 0.7$, the spanwise perturbations were suppressed as a result of higher flow velocities in the gap region, thereby leading to the flow being mainly two-dimensional and a reduction in the occurrence of dislocations. Below $G/D \le 0.53$, intermittent vortex shedding was observed. Experimental investigations at a slightly higher Reynolds number of 22 000 by Bosch et al. (1996) showed that the vortex shedding was completely suppressed at $G/D = 0.25$, while low intensity intermittent shedding occurred at higher gap ratios.

Using a finite-difference method, Lei et al. (2000) performed numerical simulations for a circular cylinder for G/D between 0.1 and 3 and for Reynolds numbers $80 \le Re \le 1000$. In their simulations, the lower wall and the cylinder were fixed and a boundary layer started $16D$ upstream of the cylinder. They observed that the gap height at which vortex shedding was suppressed decreased as the Reynolds number was increased up to $Re = 600$. Beyond this value, the critical gap height remained constant. A similar study was performed by Harichandan and Roy (2012) for a flow starting $10D$ upstream of the cylinder at $Re = 100$ and 200. Single sided vortex shedding was observed for $G/D = 0.2$ and $Re = 200$, and as the gap height was increased, Kármán type shedding was observed.

One of the earliest visualisations of the wake of a circular cylinder moving parallel to a wall was by Taneda (1965), who visualised the vortex streets for the cylinder moving at gap heights of $G/D = 0.6$ and 0.1 at $Re = 170$. For $G/D = 0.1$, a single row of vortices formed and these were unstable and dissipated quickly. Furthermore, the wavelength of vortex street increased as the gap ratio was decreased.

Nishino et al. (2007) performed experimental investigations for a circular cylinder near a moving wall for higher Reynolds numbers ($O(10^5)$). For a cylinder with endplates, they reported that the flow essentially remained two-dimensional, with Kármán type vortices being shed for gap heights $G/D > 0.5$, and an intermediate shedding regime being observed for $0.35 \le G/D \le 0.5$, followed by complete cessation of shedding below $G/D < 0.35$. They further reported that the drag coefficient was nearly constant when the body was below $G/D < 0.35$. However, for a cylinder without endplates, they reported that the Kármán type vortices were not being generated and the drag coefficient was nearly constant in this regime.

Zerihan and Zhang (2000) investigated the variation of lift and drag forces on a single element wing (of chord c) with a moving ground in a wind tunnel at high Reynolds numbers ($O(10^4)$). For the airfoil tested, the (negative) lift coefficient increased from its value at low gap heights to a maximum value at height $h = 0.08c$, beyond which a decrease in the lift coefficient was observed. The drag coefficient decreased on increasing gap height. They further varied the incidence angle of the airfoil and observed that the gap height at which the maximum (negative) lift was generated varied marginally.

Zhang et al. (2005) investigated the ground effect of a half-cylinder using a moving ground in a wind tunnel facility for Reynolds numbers in the range $6.8 \times 10^4 \le Re \le 1.7 \times 10^5$. The critical gap height range over which vortex shedding was suppressed was found to be $0.525 \le G/D \le 0.55$. The drag force was nearly constant below this height but a sharp increase to twice the value was observed around the critical gap height. The lift coefficient decreased as the gap height was increased. Furthermore, the Strouhal number was found to be insensitive to the gap height.

Bhattacharyya and Maiti (2005) investigated the flow for a square cylinder near a moving wall for a wide range of Reynolds numbers (below 1400) for $0.1 \le G/D \le 0.5$. They observed that the mean lift coefficient decreased gradually as Reynolds number was increased, while the drag coefficient increased with Reynolds number. The lift and drag coefficients were higher for lower gap heights. They further observed that the Strouhal number decreased as the gap height was decreased. They obtained the velocity profiles in the gap between the cylinder and the wall.

Huang and Sung (2007) performed two-dimensional simulations for a circular cylinder moving near a wall for $0.1 \le G/D \le \infty$ for $Re \le 600$. The gap height at which alternate vortex shedding disappeared decreased from $0.28D$ to $0.25D$ as the Reynolds number was increased from 300 to 600. The non-dimensionalised shedding frequency (St) at different Reynolds numbers increased as the cylinder was brought closer to the wall ($\simeq 0.5D$) followed by a rapid decrease as the gap height was decreased. They further quantified the lift and drag coefficients, with the lift coefficient showing a linear increase as the cylinder was brought closer to the wall. They however did not rule out the possibility that three-dimensional effects would be important for such flows.

Using an immersed boundary technique, Yoon et al. (2010) performed numerical investigations at various gap heights for a circular cylinder moving parallel to a wall at $Re \le 200$. The time-averaged lift and drag coefficients decreased

exponentially as the gap height was increased. They observed steady flow at higher Reynolds numbers as the gap height was decreased. Vortex shedding persisted at $Re = 120$ for the cylinder with $G/D = 0.1$.

For a body moving along a wall, Arnal et al. (1991) observed that the presence of a wall had a stabilising effect on the flow dynamics, delaying the transition to unsteady flow to higher Reynolds numbers. For a square cylinder sliding along a wall, they observed that the onset of unsteady flow occurred around $Re = 100$, where the vortex pair moved away from the wall. Instabilities of this nature occurred when vortex cores convected at slower velocities than the mean flow, as shown by the experimental investigations of Lim et al. (2004) for a flat plate boundary layer. Dipankar and Sengupta (2005) further showed that the instability occurs in the convecting vortex core shed from the freestream side of the cylinder.

Mahir (2009) investigated the onset of three-dimensional flow for a square cylinder near a fixed wall for $Re \leq 250$ as the gap height was increased from 0.1 to 4. At $Re = 185$, mode A type vortex structures of spanwise wavelength $3D$ were observed for gap heights greater than $G/D = 1.2$, while at $G/D = 0.8$, mode B type vortex structures with $1D$ spanwise wavelength were observed. Below $G/D = 0.5$, neither mode A nor B type vortex structures were observed. At $Re = 250$, mode B type vortex structures were observed at larger gap heights, while at lower gap heights the vortex structure was strongly distorted in the vicinity of the cylinder. In the frequency spectra of the streamwise and spanwise velocities for $G/D = 0.8$ and $Re = 185$, period-doubling was observed.

Stewart et al. (2006, 2010b) performed numerical and experimental investigations for a circular cylinder moving near a plane wall at a very small gap height ($G/D = 0.005$) for $Re \leq 200$. They reported that the flow was steady up to $Re = 165$, beyond which periodic flow was observed, where oppositely signed vortex structures combined and self-propelled away from the wall. They further performed linear stability analysis and determined the onset of three-dimensional flow. The flow became three dimensions directly from steady flow at $Re_c = 70.5$, unlike the case for an isolated cylinder, for which the transition to a three-dimensional state occurs from the unsteady flow. Experimental wake visualisations for the cylinder near a wall in a water tunnel were in good agreement with the numerical simulations.

In this study, we perform two-dimensional simulations for a circular cylinder moving parallel to a wall at different gap heights using a spectral-element method. This is coupled with linear stability analysis to investigate the wake transitions and wake behaviour at different gap heights. The dependence of the force coefficients and the shedding frequency on Reynolds number and gap height is quantified.

2. Problem definition and methodology

The schematic representation of the cylinder moving parallel to the wall is shown in Fig. 1. A cylinder of diameter D is moving at a gap height of G from the wall. In the numerical setup, it is convenient to use a uniformly translating frame of reference centred on the cylinder. Relative to this non-accelerating frame, the fluid and the lower wall move at a uniform speed and the cylinder remains stationary. There are two controlling non-dimensional parameters: the Reynolds number, $Re = UD/\nu$, where ν is the kinematic viscosity of the fluid, and the gap ratio, G/D. For this study, the Reynolds number lies in the range $25 \leq Re \leq 200$. Computational domains were constructed for different gap heights from freestream ($G/D = \infty$, i.e., no wall) to a minimal gap ($G/D = 0.005$). The small gap was maintained to prevent a singular mesh element between the bottom of the cylinder and the lower wall. Previous studies (Rao et al., 2011; Stewart et al., 2006, 2010b) have shown good agreement between the flow structures visualised in the experiments and those observed numerically, even though the force coefficients are sensitive to gap height for small gaps. As is usual, the lift force (F_l) and drag force (F_d) are normalised by the dynamic pressure and area ($0.5\rho U^2 D$) to obtain the lift (C_L) and drag (C_D) coefficients, respectively. In the unsteady regime of flow, vortex shedding occurs and the force coefficients vary periodically, so time-averaged quantities are reported. The simulations were performed for $\tau > 400$, where time, t, is non-dimensionalised by $U/D(\tau = tU/D)$. The frequency of shedding, f, is normalised by the cylinder diameter and flow speed to obtain the non-dimensional Strouhal number, $St = fD/U$.

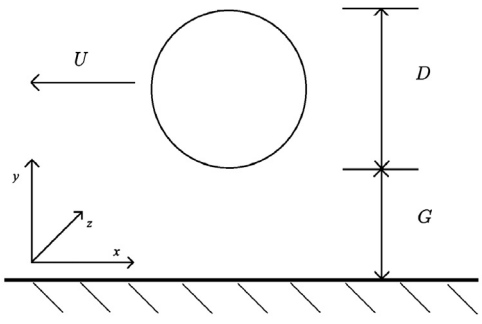

Fig. 1. Schematic representation of the circular cylinder of diameter D at a distance G from the wall.

2.1. Numerical formulation

The incompressible Navier–Stokes equations are solved using a spectral-element method. The computational domain is constructed from quadrilateral elements, mainly rectangular, while some have curved boundaries to accurately treat the curved surface of the cylinder. These elements are further subdivided into internal node points which are distributed according to the Gauss–Legendre–Lobatto quadrature points, with the velocity and pressure fields represented by tensor products of Lagrangian polynomial interpolants within the elements. Such methods are known to provide spectral convergence as the polynomial order of the interpolants is increased (Karniadakis and Sherwin, 2005). The number of node points ($N\times\ N$) is specified at runtime, with the interpolant polynomial order being $N-1$. A fractional time-stepping technique is used to integrate the advection, pressure and diffusion terms of the Navier–Stokes equation forward in time. The unsteady solver is used to investigate the parameter range covering both the steady and unsteady regimes of flow. More details on this method can be found in Thompson et al. (2006a) and has previously been used in studies of bluff bodies in freestream (Leontini et al., 2007; Thompson et al., 1996, 2006b), for bodies near a wall (Rao et al., 2011; Stewart et al., 2006, 2010a, 2010b; Thompson et al., 2007) and for bodies in a confined flow (Griffith et al., 2007, 2011).

2.2. Linear stability analysis

For an isolated cylinder, three-dimensional flow occurs for $\mathrm{Re}\gtrsim 190$ (Barkley and Henderson, 1996; Williamson, 1996a, 1996b) in the unsteady regime, while for bodies close to a wall the flow becomes three-dimensional directly from a steady base flow (Rao et al., 2011; Stewart et al., 2010b). We here investigate the variation between these two extremes mapping the transition for different gap heights. The bifurcation to three-dimensional flow is determined using linear stability analysis. Numerically, the Navier–Stokes equations are linearised and the spanwise perturbations are constructed as a set of Fourier modes. The resulting equations are marched forward in time, and after several periods, the fastest growing or slowest decaying modes dominate the system. For unsteady (periodic) flows, the analysis is based on the growth over a base flow period (T) and is known as Floquet analysis. In that case, the ratio of the amplitudes of the perturbation field for consecutive periods is denoted by $\mu=e^{\sigma T}$, where μ is the Floquet multiplier or the amplification factor and σ is the growth rate. For exponentially growing modes, the Floquet multiplier returns a value of $|\mu|>1$, or a positive growth rate ($\mathrm{Re}(\sigma)>0$). For a circular cylinder, the fastest growing modes at the onset of three-dimensionality have a purely real Floquet multiplier, i.e., the periodicity of the three-dimensional perturbations is the same as the base flow period. However, other unstable modes which are incommensurate with the base flow also occur, e.g., for a circular cylinder (Blackburn and Lopez, 2003), square cylinder (Robichaux et al., 1999) or flat plate (Thompson et al., 2006b). In addition, it is also possible for the perturbation modes to have twice the period of the base flow such as for the wake behind rings Sheard et al. (2003, 2004) and inclined square cylinders in freestream (Sheard, 2011; Sheard et al., 2009). These are termed sub-harmonic modes.

Details of the approach can be found in, e.g., Ryan et al. (2005) and Leontini et al. (2007).

2.3. Resolution studies

The domain used for the two-dimensional flow computations had boundaries positioned at large distances from the cylinder-wall system to minimise blockage. The inlet and outlet boundaries were placed $100D$ from the cylinder, while the transverse boundary was located $150D$ from the lower wall. Studies conducted by Rao et al. (2011) showed negligible changes to the force coefficients and Strouhal number if larger domains were used. Furthermore, spatial resolution studies were conducted for $G/D=0.01$ at $\mathrm{Re}=200$ by varying the number on internal nodes within each element ($N\times N$), between $N^2=4^2$ and 10^2. For $N^2=7^2$, maximum variation in the force coefficients and Strouhal number from the most highly resolved case was less than 0.1%. However, because the macro-element mesh resolution is considerably lower away from the solid surfaces, to ensure adequate resolution of the flow structures in the far wake the internal resolution was set to $N^2=9^2$. Further, to ensure stability of the solver at these resolutions, which is governed by a Courant condition for the explicit non-linear sub-step, the time-step used was 0.001.

3. Results

3.1. Flow structures

The parameter investigation was carried out between $G/D=0.005$ and $G/D\to\infty$ for Reynolds numbers $25\leq\mathrm{Re}\leq 200$. The flow for all cases investigated is steady at low Reynolds numbers and is characterised by the formation of recirculation zones behind the cylinder. For small gap heights, a single recirculation zone forms in the wake away from the wall, and as the gap height is increased, the formation of a secondary recirculation can be observed as the wake becomes more symmetrical. In line with the isolated cylinder case, the length of these recirculation zones increases as the Reynolds number is increased. At still higher Reynolds numbers, the flow undergoes transition to an unsteady state, with the wake state is characterised by the periodic shedding of vortices. For bodies close to the wall ($G/D\leq 0.1$), the critical Reynolds number for transition to an unsteady state was higher than $\mathrm{Re}=165$, and as the gap height was increased, the unsteady

transition occurred at lower Reynolds numbers. Recall that for bodies near a wall, three-dimensional flow occurs in the steady regime of flow (Stewart et al., 2010b). For bodies close to a wall, vortex shedding occurs when the negatively signed separating shear layer from the top of the cylinder combines with oppositely signed vorticity from the boundary layer at the wall to form vortex pairs, which self-propel away from the wall. However, for the cylinder moving at larger gap heights, the unsteady wake is characterised by the formation of the classical von Kármán vortex street. Shown in Fig. 2 are the coloured vorticity contour plots for the cylinder moving at different gap heights above the wall at Re = 200. The images shown are at instant of maximum lift coefficient in the shedding cycle.

The variation of the time-averaged drag and lift coefficients is shown in Fig. 3 in the steady regime of flow. Studies by Stewart et al. (2010b) show that the drag coefficient obeys a power law relationship with Reynolds number. Shown here on a log–log plot, the drag coefficient varies approximately linearly in the steady regime. There is a difference in the drag coefficient of approximately 2 between the smallest and largest gap cases. The mean lift coefficient varies substantially more since the mean lift approaches zero as $G/D \to \infty$.

The variation of the time-averaged drag and lift coefficients together with the standard deviations is shown in Fig. 4 for the unsteady regime of flow. Over this Reynolds number range the mean drag coefficient changes only by approximately 10% or less as the gap ratio or Reynolds number is varied.

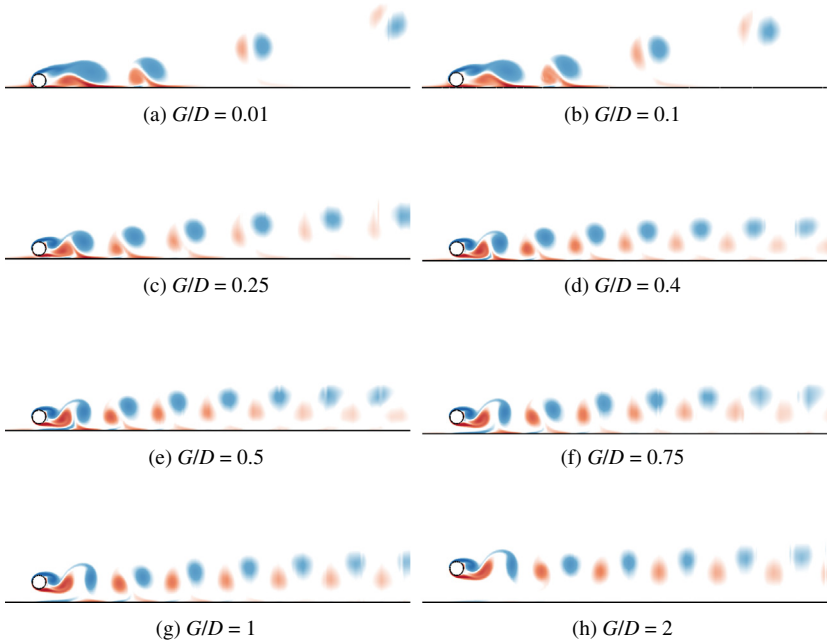

Fig. 2. Flow structures at Re = 200 for the circular cylinder moving from right to left at the specified gap heights. Vorticity contour levels are between $\pm 5D/U$. The wake is visualised for a streamwise distance in excess of $25D$ downstream of the cylinder. (For interpretation of the references to color in this figure legend, the reader is referred to the web version of this article.)

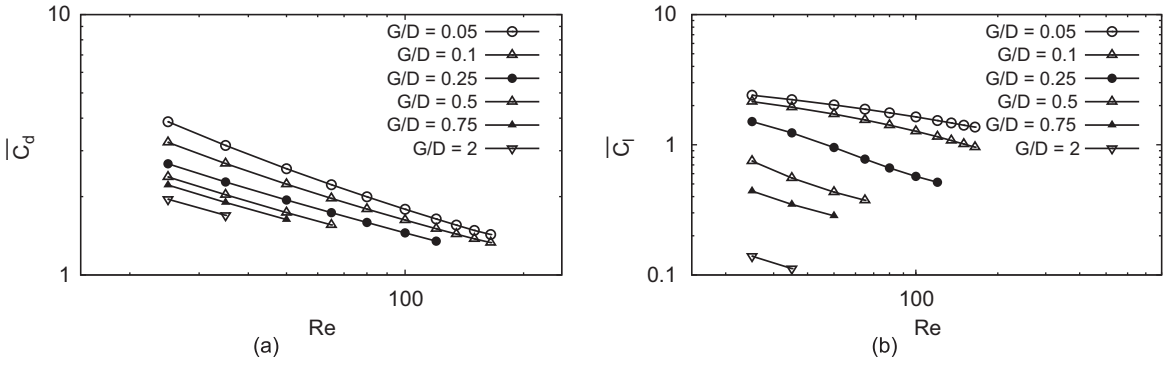

Fig. 3. Variation of the drag (a) and lift (b) coefficients with Reynolds numbers for the gap heights shown. The flow is steady for these parameters.

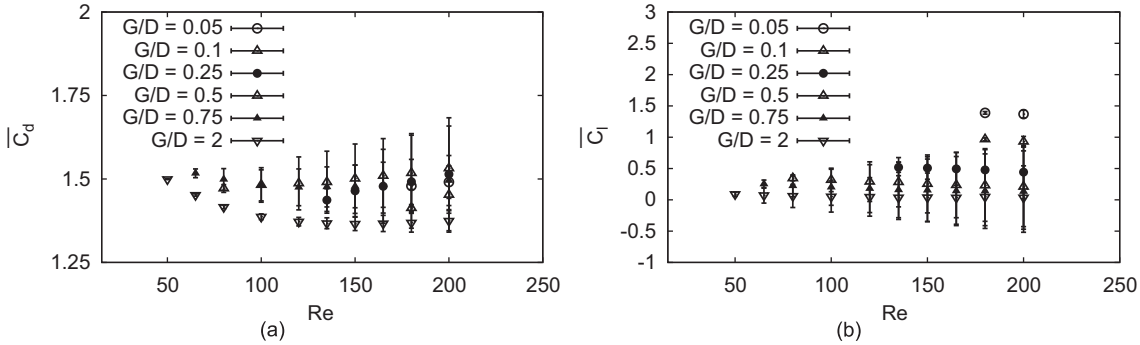

Fig. 4. Variation of the force coefficients with Reynolds numbers in the unsteady regime for the gap heights shown. The error bars represent one standard deviation from the mean values.

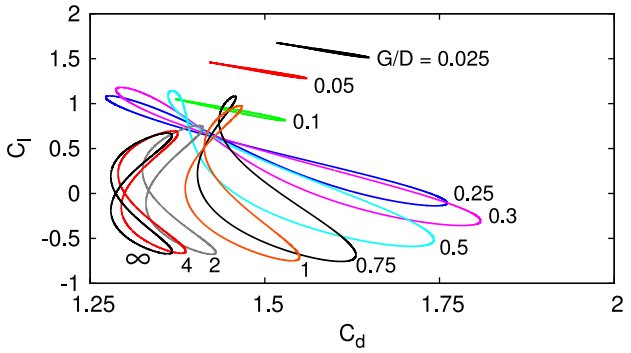

Fig. 5. Force coefficient phase trajectories at different gap heights for periodic flow at Re=200.

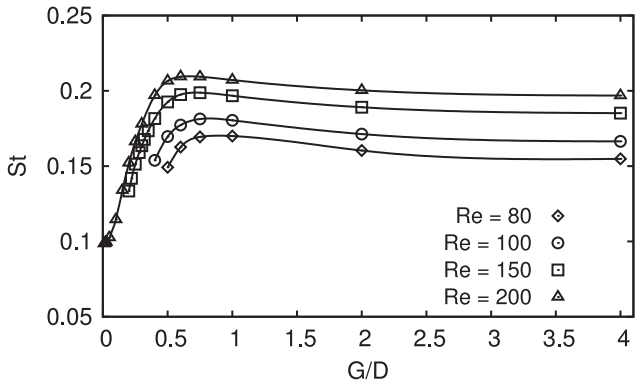

Fig. 6. Variation of Strouhal number with gap height for different Reynolds numbers.

Phase diagrams for various gap heights are provided in Fig. 5 at Re=200. C_l is plotted against C_d at each gap height. The curves show the phase relationship between the force coefficients and the variation of the amplitude over one period of the lift coefficient. For $G/D=\infty$, the phase relationship is symmetric between two halves of the cycle, and an apparent loss in symmetry is observed for $G/D\leq 1$. For very small gaps ($G/D\leq 0.1$), the shedding becomes substantially one-sided, as shown in Fig. 2, where the lift and drag signals are out of phase by approximately 180°.

The variation of the shedding frequency (St) with gap height for various Reynolds numbers is shown in Fig. 6. The Strouhal number drops substantially as the cylinder is positioned closer to the wall, approaching a value of approximately 0.1 as the gap approaches zero. As the gap height is increased, the Strouhal number increases almost linearly initially before reaching a maximum for $0.5\leq G/D\leq 0.75$, above which it decreases slightly as it asymptotes to the value for an isolated cylinder in freestream. Predictions from Huang and Sung (2007) and an independent immersed boundary code (J.S. Leontini, private

communication) are in good agreement with the current Strouhal number predictions. It is also interesting that a similar decrease in Strouhal number is found when a cylinder approaches a free surface (Reichl et al., 2005).

3.2. Stability analysis

The stability of the flow to spanwise perturbations is investigated for cylinders moving at different gap heights above the wall. Two-dimensional steady or unsteady flow solutions are used to provide base flows to investigate the stability to three-dimensional perturbations.

For $G/D=\infty$, Barkley and Henderson (1996) showed that the flow became linearly unstable to three-dimensional perturbations at $\mathrm{Re}_c=188.5$ for $\lambda_c/D=3.96$. Our stability analysis performed on the unsteady base flow showed that for this case the flow becomes unstable at $\mathrm{Re}_c=190.5$ for the same spanwise wavelength. The marginal variation in the critical Reynolds number between these two predictions (O(1%)) can be attributed to the considerably larger domain size used here, which also leads to a slightly different Strouhal number to that found by Barkley and Henderson (1996). Stability analysis performed on the steady base flow at $G/D=0.005$ (Rao et al., 2011) is in agreement with the previous studies of Stewart et al. (2010b). The current investigation was carried out to quantify the variation with gap height, mapping the boundary between the two- and three-dimensional regimes.

The variation of the critical spanwise wavelength and critical Reynolds number with gap height is shown in Fig. 7 for gap heights $G/D\leq 1.2$. In Fig. 7(a), the approximate demarcation between the steady and unsteady regimes is shown by the dotted line.

For $G/D\leq 0.22$, stability analysis was performed on a steady base flow, where the power method was used to resolve the dominant growing mode. However, for gap heights greater than $G/D=0.22$, stability analysis was performed on an unsteady base flow using the Arnoldi method to resolve the dominant Floquet modes based on Krylov subspace iterates. This method can resolve both the real and imaginary components of the Floquet multiplier of the first few most-dominant modes. Domains used for the computations of the steady base flow were used for the stability analysis for the steady regime, while the computational domain had to be resized for the analysis in the unsteady regime. In that case, the perturbation fields were not adequately resolved in the far wake ($x/D>30$), where the macro-elements are large. Since the modes are global modes (with the same growth rate everywhere), inadequate resolution, such as in the far wake, can lead to spurious growth rate predictions if unphysical large mode amplitudes occur there. To combat this problem, new computational domains were constructed with boundaries closer to the cylinder. The Strouhal numbers for the smaller domains were computed. The variation in the Strouhal number values between the larger and smaller sized domains was $\simeq 15\%$. Although this will affect the accuracy of critical Reynolds numbers and growth rates by a similar percentage, it is unlikely to affect the underlying physics.

Fig. 8 shows the computed spanwise perturbation vorticity contours for the most unstable wavelengths near the critical Reynolds numbers for onset of the instability. Spanwise vorticity contours of the base flow are overlaid to highlight the relative position of high mode amplitudes. This instability contours resemble those for a backward-facing step (Blackburn et al., 2008), flow downstream of a blockage or sudden expansion (Griffith et al., 2007, 2008; Marquet et al., 2008) or even the instability in the flow over a forward-facing blunt plate (Thompson, 2012). Those cases have in common an attached downstream recirculation zone, and lead to a large spanwise-wavelength steady three-dimensional instability, which generates recirculating flows in the horizontal (x–y) plane.

At $G/D=0.28$, the flow remained two-dimensional for $\mathrm{Re}\leq 200$. For larger gap ratios ($G/D\gtrsim 0.3$), the three-dimensional instability first manifests after the flow has already become unsteady. This case is analogous to Mode A for an isolated circular cylinder, with the critical Reynolds number and wavelength curves shown in Fig. 7 indicating a continuous transition towards the corresponding Mode A values. The mode structures for different gap heights are shown

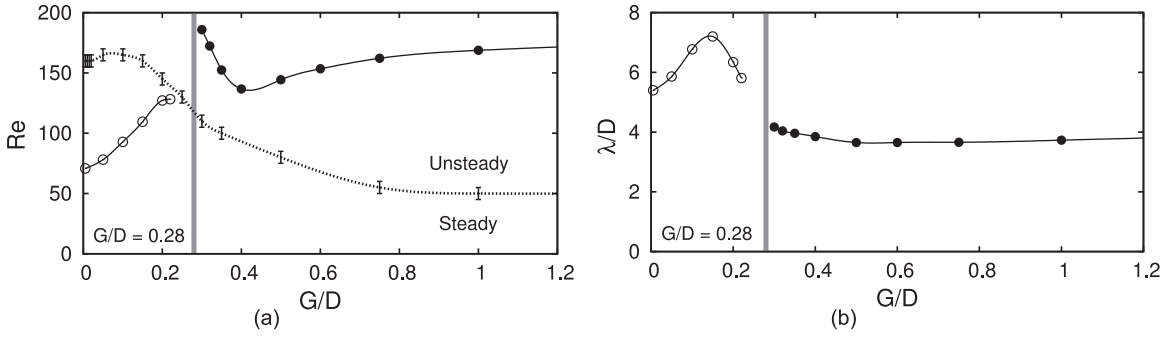

Fig. 7. Variation of critical values for the onset of three-dimensional flow with gap height. (a) Variation of the critical Reynolds number with G/D. The boundary of the transition between the steady and unsteady regimes obtained using a two-dimensional base flow is shown by the dotted line. (b) Variation of the critical spanwise wavelength with G/D. The three-dimensional modes which grow on the steady base flow are marked by open circles (○) and those on the unsteady base flow by filled circles (•). In each diagram, the gap height at which the flow is stable to three-dimensional perturbations for $\mathrm{Re}\leq 200$ is shown by the vertical grey line.

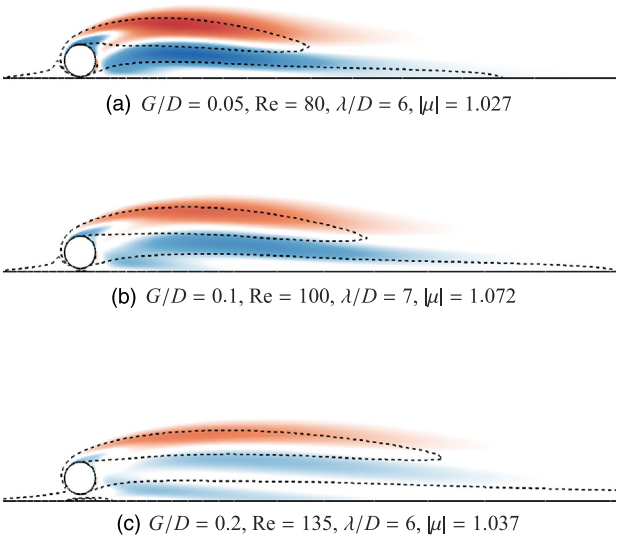

(a) $G/D = 0.05$, Re = 80, $\lambda/D = 6$, $|\mu| = 1.027$

(b) $G/D = 0.1$, Re = 100, $\lambda/D = 7$, $|\mu| = 1.072$

(c) $G/D = 0.2$, Re = 135, $\lambda/D = 6$, $|\mu| = 1.037$

Fig. 8. Spanwise perturbation vorticity colour contours (between levels $\pm 0.1D/U$) for the cylinder moving at different gap heights at the specified Reynolds number and spanwise wavelength. Base flow vorticity contours between levels $\pm 1D/U$ are overlaid. The cylinder is moving from right to left in each image. (For interpretation of the references to color in this figure legend, the reader is referred to the web version of this article.)

in Fig. 9, highlighting the broad similarities in the perturbation fields. In particular, the near wake shows high perturbation amplitude in the forming vortex cores as well as in the sheared region between the cores, and further downstream the perturbation is high in the vortex cores and drops to zero at the edge, reminiscent of the perturbation field structure for an elliptic instability as found for mode A, e.g., Thompson et al. (2001) and Leweke and Williamson (1998). Although for small gap heights there is some interaction with the no-slip wall contributing to the mode structure, this does not dominate the evolving perturbation field.

Table 1 provides the critical values of Reynolds number and spanwise wavelength for the three-dimensional transition as a function of the gap height.

3.3. *Stability analysis at higher Reynolds numbers for bodies near a wall*

Previous studies by Rao et al. (2011) and Stewart et al. (2010b) reported three-dimensional flow in the steady regime at low Reynolds numbers prior to the onset of unsteady flow for a circular cylinder near a wall. Barkley and Henderson (1996) performed stability analysis at $\mathrm{Re} = 280$ for an isolated cylinder and observed a short wavelength instability, commonly known as mode B. Here, we perform a similar analysis to predict all the amplified growing modes at a higher Reynolds numbers well past the transition value, and then we use three-dimensional direct numerical simulations to further investigate the nature of the saturated wake state.

For a cylinder (effectively) sliding along a wall ($G/D = 0.005$), the two-dimensional flow undergoes transition to an unsteady wake state at $\mathrm{Re} \simeq 160$. Stability analysis was performed on the unsteady base flow at $\mathrm{Re} = 200$ to obtain the fastest growing modes. The growth rate curves are shown in Fig. 10. Four distinct modes are observed for $\lambda/D \leq 25$, with the shortest wavelength mode at $\lambda/D = 2.4$ (termed mode I) being the fastest growing. Three other modes whose maximum growth rate peaks are at $\lambda/D = 4.55, 5.35$ and 11 and are termed mode II, mode III and mode IV, respectively. The corresponding spanwise perturbation vorticity fields at these preferred spanwise wavelengths are shown in Fig. 11.

To further investigate the nature of these modes, the real and imaginary components of the resulting Floquet multipliers are resolved. These are plotted in the complex plane for each of the four modes in Fig. 12. The horizontal and the vertical axis correspond to the real and imaginary components of the Floquet multipliers, respectively. The unit circle ($|\mu| = 1$) is shown by the solid line. This separates the region where perturbations decay (inside the circle) from where perturbations grow (outside the circle). Modes I, III and IV were found to be quasi-periodic, i.e., the period of the mode is not commensurate with that of the base flow. Mode II, on the other hand, as a purely real and negative Floquet multiplier, which indicates that it is subharmonic.

To validate the results of the stability analysis and to investigate the evolution towards a saturated wake state, we performed a three-dimensional direct numerical simulation. This was initialised from the two-dimensional periodic flow for $\mathrm{Re} = 200$, using a three-dimensional version of the computational code employing a Fourier expansion in the spanwise direction (Karniadakis and Triantafyllou, 1992; Leontini et al., 2007; Ryan et al., 2005; Thompson et al., 1996). Low intensity white noise ($O(10^{-4})$) was added to trigger the development of three-dimensional flow. The selection of the

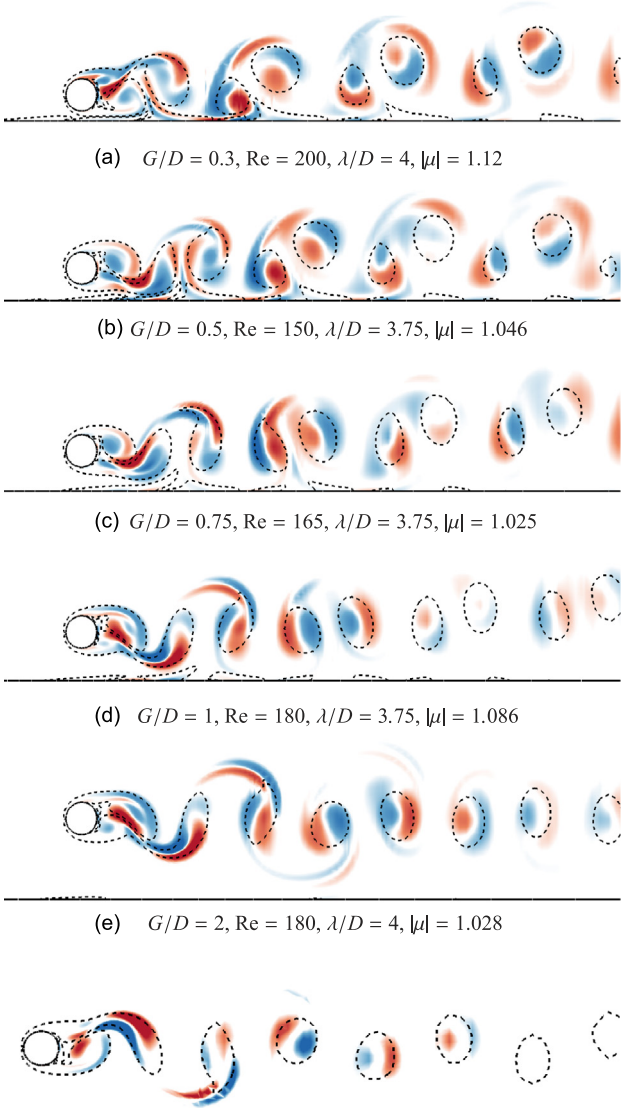

Fig. 9. Spanwise perturbation vorticity contours at the specified gap heights. The contour shading is as per Fig. 8.

spanwise domain size restricts the number of wavelengths of each of the modes that can fit into the domain to discrete values. Here, this length was chosen as 12*D*, sufficient to contain 5, 3, 2 and 1 modes I, II, III and IV wavelengths, respectively. In addition, 64 Fourier planes were used for this simulation. While this is clearly a compromise, it is sufficient to verify the initial linear evolution of the fastest growing perturbation mode, and it likely to give an idea of the complex evolution towards the asymptotic wake state as the different modes grow towards saturation and interact non-linearly.

Fig. 13(a) and (b) shows time traces of the *u* and *w* velocity components at a point in the wake as the perturbed two-dimensional flow evolves towards a three-dimensional state. These plots show that the two-dimensional state is maintained for more than 100 non-dimensional time units. Beyond approximately 160 time units, the periodicity in the *u* trace effectively disappears as strong spanwise flow develops. Fig. 13(c) is a depiction of mode I from the linear stability analysis using isosurfaces of positive and negative streamwise vorticity to indicate the wake structure. This should be compared with the DNS isosurfaces shown in Fig. 13(d), which correspond to $\tau = 95$, while mode I is still undergoing exponential amplification. This relative time is shown by the first filled circles in Fig. 13(a) and (b). Fig. 13(e) shows the complex nature of the wake at a later time ($\tau = 240$) after the wake has become highly non-linear. As indicated above, in this state even the remnants of periodicity in the *u* velocity component are lost. Also, there does not appear to be a clearly

Table 1
Variation of λ_c/D and Re_c with G/D. For $G/D \leq 0.22$, stability analysis was performed on the steady base flow and for $G/D \geq 0.25$, the linear stability analysis was performed on the periodic base flow.

G/D	λ_c/D	Re_c
0.005	5.48	70.91
0.05	5.86	78.07
0.1	6.77	92.85
0.15	7.27	109.55
0.2	6.34	127.20
0.22	5.81	128.23
0.25	5.24	128.11
0.3	4.17	185.90
0.32	4.04	172.30
0.35	3.96	152.45
0.4	3.85	136.68
0.5	3.65	144.39
0.6	3.65	153.45
0.75	3.66	162.16
1	3.73	168.75
2	3.98	177.48
4	4.03	181.22
∞	3.96	190.5

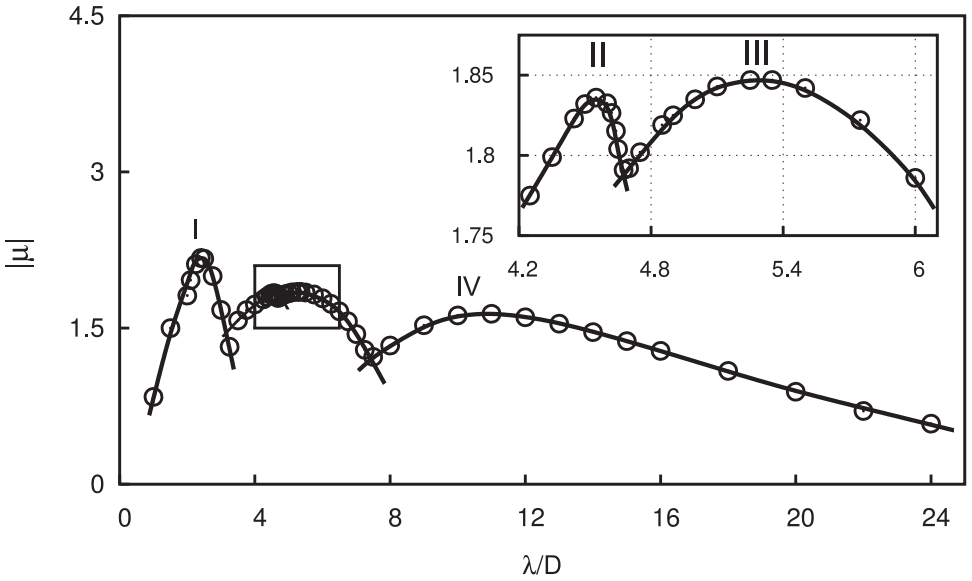

Fig. 10. Growth of the linear wake modes for the circular cylinder sliding along a wall at $\mathrm{Re} = 200$. The inset shows the two modes between $4 \leq \lambda/D \leq 6$.

dominant spanwise wavelength. In any case, the two-dimensional base flow is clearly no longer an adequate model of the real flow in this regime.

4. Conclusions

We have investigated the flow past a circular cylinder translating parallel to a no-slip wall at different gap heights. Two-dimensional simulations show the onset of unsteady flow is delayed to much higher Reynolds numbers relative to the isolated cylinder as the gap height is decreased. For a given gap height, the Strouhal number increased with Reynolds number. The force coefficients at various gap heights have been computed. The critical Reynolds numbers and spanwise wavelengths for the onset of three-dimensional flow are established as the gap height is varied. For $G/D \leq 0.22$, the onset of three-dimensional flow occurs in the steady flow regime. Beyond this, three-dimensional flow develops from unsteady

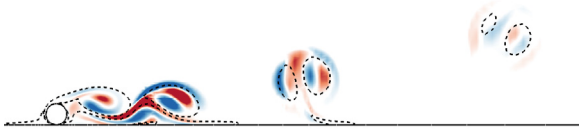

(a) mode I, $\lambda/D = 2.4$, $|\mu| = 2.174$

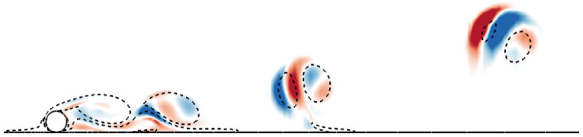

(b) mode II, $\lambda/D = 4.55$, $|\mu| = 1.836$

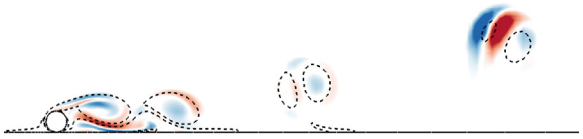

(c) mode III, $\lambda/D = 5.35$, $|\mu| = 1.8476$

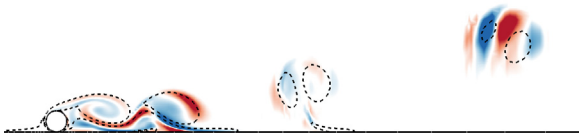

(d) mode IV, $\lambda/D = 11$, $|\mu| = 1.638$

Fig. 11. Spanwise perturbation vorticity contours for the cylinder sliding along a wall ($G/D = 0.005$) at $\mathrm{Re} = 200$. The cylinder is travelling from right to left in each image. The contour shading is as per Fig. 8.

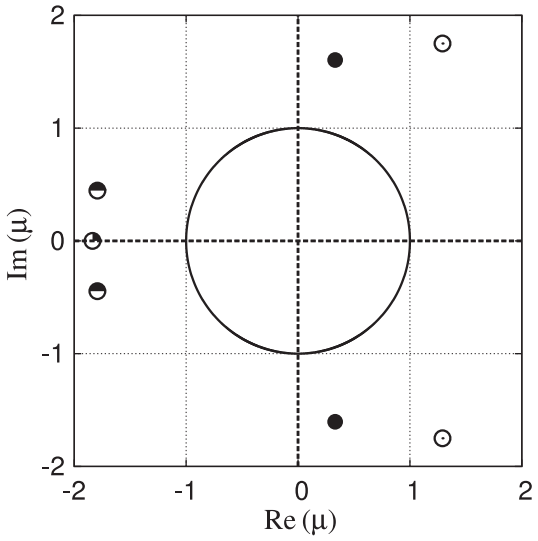

Fig. 12. The Floquet multipliers for each of the four unstable modes at $\mathrm{Re} = 200$. The modes and their conjugate pairs (if they exist) are shown along with the unit circle ($|\mu| = 1$). Mode I is shown by open circles ($\lambda/D = 2.4$), mode II is shown by quarter filled circles ($\lambda/D = 4.55$), mode III is shown by half filled circles ($\lambda/D = 5.35$) and mode IV is shown by fully filled circles ($\lambda/D = 11$).

two-dimensional flow at considerably higher Reynolds numbers (e.g., $\mathrm{Re}_c = 185$ at $G/D = 0.3$; $\mathrm{Re}_c \simeq 137$ at $G/D = 0.4$), before moving towards values approaching those observed for an isolated cylinder ($\mathrm{Re}_c = 190.5$ and $\lambda/D = 3.96$). The wake development for a Reynolds number well in excess of the initial critical value was also investigated for the lowest gap

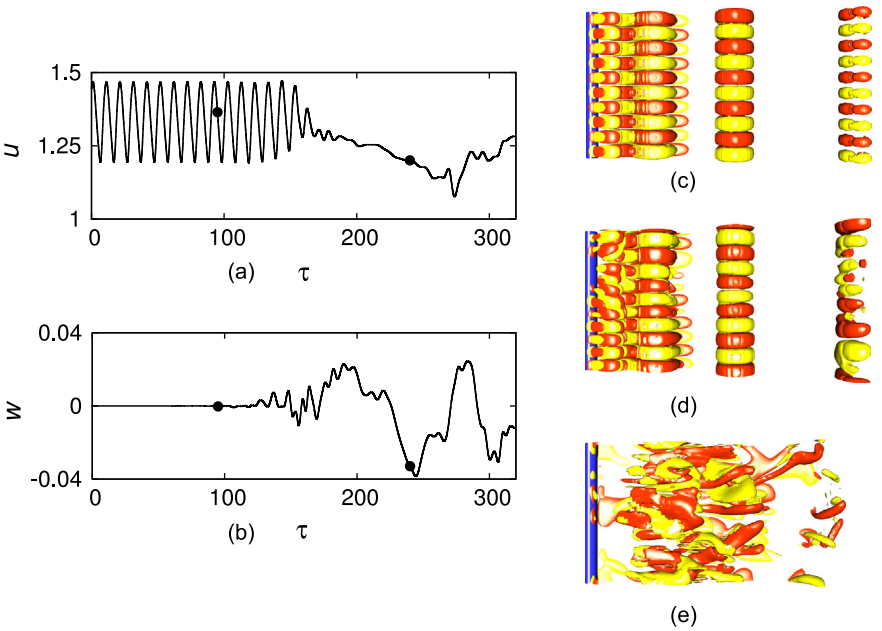

Fig. 13. Direct numerical simulation (DNS) results for a circular cylinder sliding along a wall at $\mathrm{Re}=200$. Left: The time histories of the streamwise and spanwise velocity components for a location in the wake downstream of the cylinder. Right: Visualisations using streamwise vorticity isosurfaces viewed from above. Here (c) shows isosurfaces for $\lambda/D=2.4$ from linear stability analysis, which can be compared with the perturbation field obtained from DNS at $\tau=95$ in image (d). The final image (e) shows perturbation isosurfaces at $\tau=240$ after the wake has become chaotic.

height case, $G/D=0.005$, effectively a cylinder sliding along a wall. At $\mathrm{Re}=200$, Floquet analysis shows that the two-dimensional periodic wake is unstable to four different instability modes. The evolution of the wake was followed using DNS for this case as the initially two-dimensional weakly perturbed flow evolves towards its asymptotic state. This simulation shows that initial development of the fastest growing mode, in agreement with the stability analysis, and subsequent rapid transition to a chaotic wake state, for which even quasi-periodic shedding of two-dimensional rollers into the wake seems to be suppressed.

Acknowledgements

The support from Australian Research Council Discovery Grants DP0877327 and DP0877517 and computing time from the National Computational Infrastructure (NCI), Victorian Life Sciences Computation Initiative (VLSCI) and Monash Sungrid are gratefully acknowledged. A.R. also acknowledges the support of a Monash University Departmental Postgraduate Scholarship. We also thank J.S. Leontini for his assistance in validating some of our results using an immersed boundary code.

References

Arnal, M., Goering, D., Humphrey, J.A.C., 1991. Vortex shedding from a bluff body adjacent to a plane sliding wall. ASME Journal of Fluids Engineering 113, 384–398.

Bailey, S., Martinuzzi, R., Kopp, G., 2002. The effects of wall proximity on vortex shedding from a square cylinder: three-dimensional effects. Physics of Fluids 14, 4160–4177.

Barkley, D., Henderson, R.D., 1996. Three-dimensional Floquet stability analysis of the wake of a circular cylinder. Journal of Fluid Mechanics 322, 215–241.

Bearman, P.W., Zdravkovich, M.M., 1978. Flow around a circular cylinder near a plane boundary. Journal of Fluid Mechanics 89, 33–47.

Bhattacharyya, S., Maiti, D.K., 2005. Vortex shedding from a square cylinder in presence of a moving wall. International Journal for Numerical Methods in Fluids 48, 985–1000.

Blackburn, H.M., Barkley, D., Sherwin, S.J., 2008. Convective instability and transient growth in flow over a backward-facing step. Journal of Fluid Mechanics 603, 271–304.

Blackburn, H.M., Lopez, J.M., 2003. On three-dimensional quasiperiodic Floquet instabilities of two-dimensional bluff body wakes. Physics of Fluids 15, L57–L60.

Bosch, G., Kappler, M., Rodi, W., 1996. Experiments on the flow past a square cylinder placed near a wall. Experimental Thermal and Fluid Science 13, 292–305.

Dipankar, A., Sengupta, T.K., 2005. Flow past a circular cylinder in the vicinity of a plane wall. Journal of Fluids and Structures 20, 403–423.

Griffith, M.D., Leontini, J., Thompson, M.C., Hourigan, K., 2011. Vortex shedding and three-dimensional behaviour of flow past a cylinder confined in a channel. Journal of Fluids and Structures 27, 855–860.

Griffith, M.D., Leweke, T., Thompson, M.C., Hourigan, K., 2008. Steady inlet flow in stenotic geometries: convective and absolute instabilities. Journal of Fluid Mechanics 616, 111–133.
Griffith, M.D., Thompson, M.C., Leweke, T., Hourigan, K., Anderson, W.P., 2007. Wake behaviour and instability of flow through a partially blocked channel. Journal of Fluid Mechanics 582, 319–340.
Harichandan, A.B., Roy, A., 2012. Numerical investigation of flow past single and tandem cylindrical bodies in the vicinity of a plane wall. Journal of Fluids and Structures 33, 19–43.
Henderson, R., 1997. Nonlinear dynamics and pattern formation in turbulent wake transition. Journal of Fluid Mechanics 352, 65–112.
Huang, W.X., Sung, H.J., 2007. Vortex shedding from a circular cylinder near a moving wall. Journal of Fluids and Structures 23, 1064–1076.
Karniadakis, G.E., Sherwin, S.J., 2005. Spectral/hp Methods for Computational Fluid Dynamics. Oxford University Press, Oxford.
Karniadakis, G.E., Triantafyllou, G.S., 1992. Three-dimensional dynamics and transition to turbulence in the wake of bluff objects. Journal of Fluid Mechanics 238, 1–30.
Lei, C., Cheng, L., Armfield, S., Kavanagh, K., 2000. Vortex shedding suppression for flow over a circular cylinder near a plane boundary. Ocean Engineering 27, 1109–1127.
Leontini, J.S., Thompson, M.C., Hourigan, K., 2007. Three-dimensional transition in the wake of a transversely oscillating cylinder. Journal of Fluid Mechanics 577, 79–104.
Leweke, T., Williamson, C.H.K., 1998. Three-dimensional instabilities in wake transition. European Journal of Mechanics B/Fluids 17, 571–586.
Lim, T.T., Sengupta, T.K., Chattopadhyay, M., 2004. A visual study of vortex-induced subcritical instability on a flat plate laminar boundary layer. Experiments in Fluids 37, 47–55.
Mahir, N., 2009. Three-dimensional flow around a square cylinder near a wall. Ocean Engineering 36, 357–367.
Marquet, O., Sipp, D., Chomaz, J.M., Jacquin, L., 2008. Amplifier and resonator dynamics of a low-Reynolds-number recirculation bubble in a global framework. Journal of Fluid Mechanics 605, 429.
Nishino, T., Roberts, G., Zhang, X., 2007. Vortex shedding from a circular cylinder near a moving ground. Physics of Fluids 19, 025103-1–025103-12.
Price, S.J., Sumner, D., Smith, J.G., Leong, K., Païdoussis, M.P., 2002. Flow visualization around a circular cylinder near to a plane wall. Journal of Fluids and Structures 16, 175–191.
Rao, A., Stewart, B., Thompson, M., Leweke, T., Hourigan, K., 2011. Flows past rotating cylinders next to a wall. Journal of Fluids and Structures 27, 668–679.
Reichl, P., Hourigan, K., Thompson, M.C., 2005. Flow past a circular cylinder close to a free surface. Journal of Fluid Mechanics 533, 269–296.
Robichaux, J., Balachandar, S., Vanka, S.P., 1999. Three-dimensional Floquet instability of the wake of square cylinder. Physics of Fluids 11, 560–578.
Ryan, K., Thompson, M.C., Hourigan, K., 2005. Three-dimensional transition in the wake of elongated bluff bodies. Journal of Fluid Mechanics 538, 1–29.
Sheard, G.J., 2011. Wake stability features behind a square cylinder: focus on small incidence angles. Journal of Fluids and Structures 27, 734–742.
Sheard, G.J., Fitzgerald, M.J., Ryan, K., 2009. Cylinders with square cross-section: wake instabilities with incidence angle variation. Journal of Fluid Mechanics 630, 43–69.
Sheard, G.J., Thompson, M.C., Hourigan, K., 2003. From spheres to circular cylinders: the stability and flow structures of bluff ring wakes. Journal of Fluid Mechanics 492, 147–180.
Sheard, G.J., Thompson, M.C., Hourigan, K., 2004. From spheres to circular cylinders: non-axisymmetric transition in the flow past rings. Journal of Fluid Mechanics 506, 45–78.
Stewart, B.E., Hourigan, K., Thompson, M.C., Leweke, T., 2006. Flow dynamics and forces associated with a cylinder rolling along a wall. Physics of Fluids 18, 111701-1–111701-4.
Stewart, B.E., Thompson, M.C., Leweke, T., Hourigan, K., 2010a. Numerical and experimental studies of the rolling sphere wake. Journal of Fluid Mechanics 643, 137–162.
Stewart, B.E., Thompson, M.C., Leweke, T., Hourigan, K., 2010b. The wake behind a cylinder rolling on a wall at varying rotation rates. Journal of Fluid Mechanics 648, 225–256.
Taneda, S., 1965. Experimental investigation of vortex streets. Journal of the Physical Society of Japan 20, 1714–1721.
Thompson, M.C., 2012. Effective transition of steady flow over a square leading-edge plate. Journal of Fluid Mechanics 698, 335–357.
Thompson, M.C., Hourigan, K., Cheung, A., Leweke, T., 2006a. Hydrodynamics of a particle impact on a wall. Applied Mathematical Modelling 30, 190–196.
Thompson, M.C., Hourigan, K., Ryan, K., Sheard, G.J., 2006b. Wake transition of two-dimensional cylinders and axisymmetric bluff bodies. Journal of Fluids and Structures 22, 793–806.
Thompson, M.C., Hourigan, K., Sheridan, J., 1996. Three-dimensional instabilities in the wake of a circular cylinder. Experimental Thermal and Fluid Science 12, 190–196.
Thompson, M.C., Leweke, T., Hourigan, K., 2007. Sphere-wall collisions: vortex dynamics and stability. Journal of Fluid Mechanics 575, 121–148.
Thompson, M.C., Leweke, T., Williamson, C.H.K., 2001. The physical mechanism of transition in bluff body wakes. Journal of Fluids and Structures 15, 607–616.
Williamson, C.H.K., 1996a. Three-dimensional wake transition. Journal of Fluid Mechanics 328, 345–407.
Williamson, C.H.K., 1996b. Vortex dynamics in the cylinder wake. Annual Review of Fluid Mechanics 28, 477–539.
Yoon, H., Lee, J., Seo, J., Park, H., 2010. Characteristics for flow and heat transfer around a circular cylinder near a moving wall in wide range of low Reynolds number. International Journal of Heat and Mass Transfer 53, 5111–5120.
Zerihan, J., Zhang, X., 2000. Aerodynamics of a single element wing in ground effect. Journal of Aircraft 37, 1058–1064.
Zhang, X., Mahon, S., Willams, C., 2005. Aerodynamics of half-cylinder in ground effect. Engineering Turbulence Modelling and Measurements, vol. 5, Rodi, W., Elsevier.